THE JOURNAL OF BIOLOGICAL CHEMISTRY VOL. 288, NO. 45, pp. 32700–32707, November 8, 2013

Basic Properties of Rotary Dynamics of the Molecular Motor *Enterococcus hirae* V_1-ATPase*

Received for publication, July 31, 2013, and in revised form, September 20, 2013 Published, JBC Papers in Press, October 2, 2013, DOI 10.1074/jbc.M113.506329

Yoshihiro Minagawa[‡1], Hiroshi Ueno[§1], Mayu Hara[‡], Yoshiko Ishizuka-Katsura[¶2], Noboru Ohsawa[¶2], Takaho Terada[¶2], Mikako Shirouzu[¶2], Shigeyuki Yokoyama[¶3], Ichiro Yamato[‖], Eiro Muneyuki[§], Hiroyuki Noji[‡], Takeshi Murata[‡‡4], and Ryota Iino[‡5]**

*From the [‡]Department of Applied Chemistry, Graduate School of Engineering, The University of Tokyo, Tokyo 113-8656, the [§]Department of Physics, Faculty of Science and Engineering, Chuo University, Tokyo 112-8551, the [¶]RIKEN Systems and Structural Biology Center, Yokohama 230-0045, the [‖]Department of Biological Science and Technology, Tokyo University of Science, Tokyo 125-8585, the **Department of Chemistry, Graduate School of Science, Chiba University, Chiba 263-8522, and [‡‡]Precursory Research for Embryonic Science and Technology (PRESTO), Japan Science and Technology Agency (JST), Chiba 263-8522, Japan*

Background: The chemomechanical coupling scheme of the rotary motor V_1-ATPase is incompletely understood.
Results: *Enterococcus hirae* V_1-ATPase (EhV_1) showed 120° steps of rotation without substeps, as commonly seen with F_1-ATPase.
Conclusion: The basic properties of rotary dynamics of EhV_1 are similar to those of *Thermus thermophilus* V_1-ATPase.
Significance: This study revealed the common properties of V_1-ATPases as rotary molecular motors, distinct from those of F_1-ATPases.

V-ATPases are rotary molecular motors that generally function as proton pumps. We recently solved the crystal structures of the V_1 moiety of *Enterococcus hirae* V-ATPase (EhV_1) and proposed a model for its rotation mechanism. Here, we characterized the rotary dynamics of EhV_1 using single-molecule analysis employing a load-free probe. EhV_1 rotated in a counterclockwise direction, exhibiting two distinct rotational states, namely clear and unclear, suggesting unstable interactions between the rotor and stator. The clear state was analyzed in detail to obtain kinetic parameters. The rotation rates obeyed Michaelis-Menten kinetics with a maximal rotation rate (V_{max}) of 107 revolutions/s and a Michaelis constant (K_m) of 154 μM at 26 °C. At all ATP concentrations tested, EhV_1 showed only three pauses separated by 120°/turn, and no substeps were resolved, as was the case with *Thermus thermophilus* V_1-ATPase (TtV_1). At 10 μM ATP ($\ll K_m$), the distribution of the durations of the ATP-waiting pause fit well with a single-exponential decay function. The second-order binding rate constant for ATP was 2.3×10^6 M^{-1} s^{-1}. At 40 mM ATP ($\gg K_m$), the distribution of the durations of the catalytic pause was reproduced by a consecutive reaction with two time constants of 2.6 and 0.5 ms. These kinetic parameters were similar to those of TtV_1. Our results identify the common properties of rotary catalysis of V_1-ATPases that are distinct from those of F_1-ATPases and will further our understanding of the general mechanisms of rotary molecular motors.

V-ATPase is a rotary molecular motor that couples ion transport to ATP hydrolysis and synthesis. The main function of V-ATPase in eukaryotes is to transport protons across a membrane by using the energy derived from ATP hydrolysis (1–3). V-ATPase also catalyzes ATP synthesis, harnessing the energy of proton flow in certain eubacteria such as *Thermus thermophilus*. V-ATPases are composed of V_1-ATPase (V_1),[6] a water-soluble moiety that hydrolyzes and synthesizes ATP, and a membrane-embedded moiety (V_0) that translocates ions. The V_1 and V_0 domains are connected by a rotary shaft and peripheral stalks (1–3). The V_1 complex is composed of A, B, D, and F subunits, in which the three A and three B subunits are alternately arranged, forming a hexameric stator A_3B_3 ring (4–7). ATP hydrolysis and synthesis occur on the catalytic sites that are located at the interfaces of the A and B subunits, with the majority of the catalytic residues residing in the A subunits. The rotary shaft is composed of D and F subunits penetrating into the central cavity of the A_3B_3 ring (6, 7).

The rotation of V_1 has been visualized using optical microscopy by attachment of a probe to the rotary shaft (8–11). V_1 of *T. thermophilus* (TtV_1), which functions as an ATP synthase, rotates stepwise in a counterclockwise direction (8). The basic step size is 120°, and similar to F_1-ATPase (F_1), the water-soluble moiety of F_0F_1-ATP synthase (12), each step is coupled to the consumption of a single ATP molecule (10). Although no

* This work was supported in part by Grants-in-aid for Scientific Research 24651167 (to R. I.) and 23370047 (to T. M.) and the Target Proteins Research Program of the Ministry of Education, Culture, Sports, Science and Technology of Japan.

[1] Both authors equally contributed to this work.
[2] Present address: Div. of Structural and Synthetic Biology, RIKEN Center for Life Science Technologies, Yokohama 230-0045, Japan.
[3] Present address: RIKEN Structural Biology Laboratory, Yokohama 230-0045, Japan.
[4] To whom correspondence may be addressed: Dept. of Chemistry, Graduate School of Science, Chiba University, Chiba 263-8522, Japan. Tel.: 81-43-290-2794; Fax: 81-43-290-2794; E-mail: t.murata@faculty.chiba-u.jp.
[5] To whom correspondence may be addressed: Dept. of Applied Chemistry, Graduate School of Engineering, The University of Tokyo, Hongo 7-3-1, Bunkyo-ku, Tokyo 113-8656, Japan. Tel.: 81-3-5841-7241; Fax: 81-3-5841-1872; E-mail: iino@appchem.t.u-tokyo.ac.jp.

[6] The abbreviations used are: V_1, V_1-ATPase; V_0, V_0-ATPase; TtV_1, *T. thermophilus* V_1-ATPase; F_1, F_1-ATPase; TF_1, thermophilic *Bacillus* PS3 F_1-ATPase; EF_1, *E. coli* F_1-ATPase; EhV_1, *E. hirae* V_1-ATPase; Ni-NTA, nickel-nitrilotriacetic acid; fps, frames/s; rps, revolutions/s.

substeps have yet been resolved in the rotation of TtV_1 (10, 11), the 120° steps of F_1 from the thermophilic *Bacillus* PS3 (TF_1) and *Escherichia coli* (EF_1) have been shown to be further divided into 80° and 40° substeps and into 85° and 35° substeps, respectively (13–15). The 80° and 85° substeps are triggered by ATP binding and ADP release, whereas the 40° and 35° substeps are known to occur after ATP cleavage and release of inorganic phosphate. Accordingly, the pauses before the 80° and 85° substeps are referred to as ATP-binding (ATP-waiting) pauses, and those prior to the 40° and 35° substeps are known as catalytic pauses. As described above, the chemomechanical coupling scheme of TtV_1 appears to be distinct from that of F_1. However, to date, the stepping rotations of V_1 complexes other than TtV_1 have not been described, and the chemomechanical coupling scheme of V_1 remains unclear (9).

Enterococcus hirae V-ATPase functions as a primary ion pump, similar in nature to eukaryotic V-ATPases (16, 17). We recently solved the crystal structures of the V_1 component of *E. hirae* V-ATPase (EhV_1) and proposed a model of its rotation mechanism (6). In this study, to characterize the stepping rotation of EhV_1, we analyzed and compared the basic properties of EhV_1 rotary dynamics with those of TtV_1, TF_1, and EF_1. As was the case with TtV_1, no substeps were resolved in the rotation of EhV_1, suggesting that 120° stepping rotation without substeps is a common property of V_1 complexes.

EXPERIMENTAL PROCEDURES

Preparation of Recombinant EhV_1 and AviTag-tagged EhV_1 Expressed in E. coli—The EhV_1 holocomplex (A_3B_3DF) was expressed in *E. coli* using the expression plasmid pTR19-FABD. We synthesized a DNA fragment containing the *ntpF*, *ntpA*, *ntpB*, and *ntpD* genes (in this order) and optimized its codon usage for *E. coli* expression. This fragment was then cloned into plasmid pTR19, the expression vector for the F_0F_1-ATP synthase of thermophilic *Bacillus* PS3 (18), after which a His_6 tag was introduced at the N terminus of the A subunit by PCR to obtain plasmid pTR19-FABD. For the rotation assay, we used the pTR19-FABD-Avi, in which the AviTag biotinylation sequence (GLNDIFEAQKIEWHE) (19) was inserted between Gly-121 and Tyr-122 of the D subunit by PCR-based mutagenesis. *E. coli* BL21(DE3) cells were transformed with pTR19-FABD or pTR19-FABD-Avi and cultured in Super Broth (32 g/liter Tryptone, 20 g/liter yeast extract, and 5 g/liter sodium chloride) containing 100 μg/ml ampicillin and 2 mM isopropyl β-D-thiogalactopyranoside at 37 °C for 20 h. Cells were suspended in buffer A (20 mM potassium P_i (pH 7.0), 230 mM NaCl, and 20 mM imidazole) and disrupted by sonication. After removal of the cell debris by centrifugation at 81,000 × *g* for 20 min at 4 °C, the solution was applied to a nickel-nitrilotriacetic acid column (Ni-NTA Superflow, Qiagen). After washing with 10 column volumes of buffer A, recombinant EhV_1 or AviTag-tagged EhV_1 (AviTag-EhV_1) was eluted with buffer B (20 mM potassium P_i (pH 7.0), 50 mM NaCl, and 200 mM imidazole). The eluted fractions were concentrated with an Amicon Ultra-10K unit (Merck Millipore) and then passed through a Superdex 200 gel-filtration column (GE Healthcare) equilibrated with buffer C (20 mM MES-NaOH (pH 6.5), 100 mM NaCl, and 10% glycerol). The purified proteins were flash-frozen in liquid nitrogen and stored at −80 °C until used.

Preparation of the A_3B_3 Subcomplex—The A_3B_3 subcomplex was expressed in *E. coli* BL21(DE3) cells harboring the expression plasmid pTR19-AB. Plasmid pTR19-AB was constructed by removing the *ntpF* and *ntpD* genes from pTR19-FABD by PCR. Expression and purification of the A_3B_3 subcomplex were performed using the same procedure as described for the EhV_1 holocomplex, and purified proteins were stored at −80 °C until used.

Preparation of the DF Subcomplex—An *E. coli* cell-free protein expression system was employed to synthesize the DF subcomplex using a mixture of plasmids containing the corresponding genes. The expressed DF subcomplex was purified as described previously (6). The homogeneity of each purified subcomplex was judged by SDS-PAGE analysis. After purification, cysteine residues in the DF subcomplex were biotinylated with a 3 M excess of biotinylation reagent (biotin-$PEAC_5$-maleimide, Dojindo) in 20 mM MOPS-KOH (pH 7.0) and 150 mM NaCl at room temperature for 20 min. The reaction was quenched using 10 mM DTT. We used a mutant DF subcomplex containing two engineered cysteine residues in its D subunit (T60C/R131C), substituted using a QuikChange site-directed mutagenesis kit (Agilent Technologies), and a single endogenous cysteine residue in both D (Cys-153) and F (Cys-54) subunits. A maximum of three of these residues can be expected to react with the biotinylation reagent. Specific biotinylation of the D subunit was confirmed by Western blotting with streptavidin-alkaline phosphatase conjugate (see Fig. 1).

Preparation of Reconstituted EhV_1—Reconstituted EhV_1 was prepared as follows. Purified A_3B_3 and biotinylated DF were mixed at a 1:2 molar ratio and incubated at room temperature for 2 h. Reconstituted EhV_1 was purified using a Superdex 200 gel-filtration column equilibrated with buffer C, flash-frozen in liquid nitrogen, and stored at −80 °C until used.

Biochemical Assay—The protein concentration of EhV_1 was determined based on UV absorbance using a molar extinction coefficient of 310,910 M^{-1} cm^{-1} calculated from its amino acid sequence (ProtParam tool, ExPASy). The ATP hydrolysis rate of EhV_1 was measured using an ATP-regenerating system. The reaction mixture contained 50 mM MES-KOH (pH 6.5), 50 mM KCl, 5 mM $MgCl_2$, 2.5 mM phosphoenolpyruvate, 0.2 mg/ml NADH, 0.1 mg/ml pyruvate kinase, and 0.1 mg/ml lactate dehydrogenase in addition to various concentrations of ATP. The rate of ATP hydrolysis was monitored as the rate of NADH oxidation at times ranging from 0 to 10 s after the addition of V_1, which was measured as a decrease in the absorbance at 340 nm. All measurements were carried out at 25 ± 1 °C.

Rotation Assay—To observe ATP hydrolysis-driven rotation of EhV_1, the A_3B_3 stator ring was immobilized on a Ni-NTA-coated glass surface via a His_6 tag introduced at the N terminus of the A subunit. Streptavidin-coated 40-nm gold colloid was then attached to the biotinylated cysteine or AviTag in the rotor DF subunit as a probe. The gold colloids were prepared as described previously (20). The rotations of the gold colloid were observed at 26 ± 1 °C by an objective-type total internal reflection dark-field microscope constructed on an Olympus IX-71 inverted microscope (20). The images were recorded with a

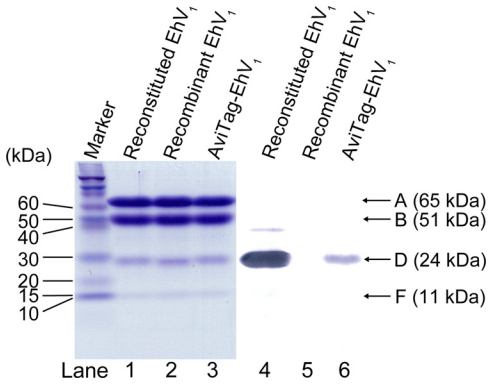

FIGURE 1. **Gel electrophoresis.** *Lanes 1–3*, SDS-PAGE of reconstituted EhV_1, recombinant EhV_1, and AviTag-EhV_1. A 16% gel was used; 12 pmol of protein was loaded in each lane. The molecular masses of the A, B, D, and F subunits are 65, 51, 24, and 11 kDa, respectively. Proteins were stained with Coomassie Brilliant Blue. *Lanes 4–6*, immunoblots stained by streptavidin-alkaline phosphatase conjugates, showing biotin labeling of the D subunit. *Lane 4*, reconstituted EhV_1 containing the biotinylated D subunit. *Lane 5*, non-biotinylated recombinant EhV_1. *Lane 6*, AviTag-EhV_1 containing the biotinylated D subunit.

high-speed CMOS camera (FASTCAM 1024PCI, Photron) at 1000–10,000 frames/s (fps). The flow cell was assembled from a Ni-NTA-coated glass (24 × 36 mm^2) and an uncoated cover glass (18 × 18 mm^2) separated by two spacers of ~50 μm thickness. First, buffer D (5 mg/ml BSA, 20 mM potassium P_i (pH 7.0), 230 mM NaCl, and 20 mM imidazole) was infused into the flow cell to prevent nonspecific binding of EhV_1 and gold colloid. After incubation for 10 min, EhV_1 (0.5–2 nM in buffer D) was infused into the flow cell. After incubation for 5 min, unbound EhV_1 was washed out with buffer D, after which gold colloid suspended in buffer D was infused. After 10 min, unbound gold colloid was washed out. Observation of rotation was initiated after infusion of buffer E (50 mM MES-KOH (pH 6.5), 50 mM KCl, and 5 mM $MgCl_2$) containing ATP (10 μM to 3 mM) or MgATP (4 and 40 mM) and an ATP-regenerating system.

RESULTS

Recombinant EhV_1—We first tried to carry out a rotation assay using recombinant EhV_1 (A_3B_3DF complex) expressed in *E. coli*. To observe the rotation, the rotation probe must be attached to the rotor DF subunits through biotin-streptavidin linkage. Because three endogenous cysteine residues in the stator A subunit (Cys-28, Cys-174, and Cys-259) may react with the biotinylation reagent, we substituted these residues with serine or alanine (C28A/C174S/C259S) and measured the activity of this mutant. The ATP hydrolysis rate of the EhV_1 mutant, measured by a biochemical assay, was <10% of that of wild-type EhV_1 (data not shown), indicating that the effect of substitution was significant.

Reconstituted EhV_1—Because the rotor DF subunit can be biotinylated separately from the stator A_3B_3 ring prior to reconstitution, we next used reconstituted EhV_1 in the rotation assay. Reconstituted EhV_1 has also been used recently for crystal structural analysis requiring a pure homogeneous sample (6). No differences were observed in the subunit composition for reconstituted EhV_1 and recombinant EhV_1 (Fig. 1), indicating a high reconstitution efficiency. Furthermore, reconstituted EhV_1 had an ATP hydrolysis rate comparable to that of recombinant EhV_1 at all ATP concentrations used, ranging from 10 μM to 4 mM (Fig. 2). The expected rotation rates of reconstituted EhV_1 and recombinant EhV_1, calculated as one-third of the ATP hydrolysis rates, followed Michaelis-Menten kinetics. The maximal rotation rate (V_{max}) and Michaelis constant (K_m) were 73 ± 2 revolutions/s (rps) and 221 ± 17 μM, respectively, for reconstituted EhV_1 and 72 ± 1 rps and 246 ± 16 μM (mean ± S.E. of fitting), respectively, for recombinant EhV_1 (Fig. 2*B*, *upper panel*, *red* and *blue dashed lines*). These results indicate that the kinetic parameters of reconstituted EhV_1 are almost identical to those of recombinant EhV_1, suggesting that the catalytic properties of EhV_1 are not affected by the reconstitution process. Therefore, we decided to use reconstituted EhV_1 for the rotation assay.

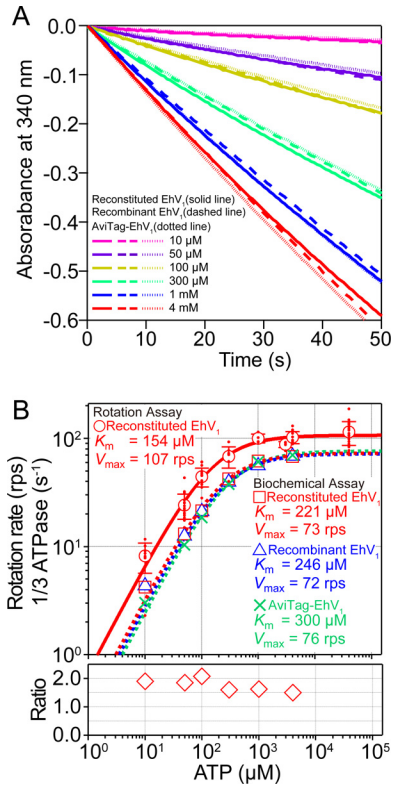

FIGURE 2. **ATP dependence of ATP hydrolysis rate and rotation rate.** *A*, time course of ATP hydrolysis by reconstituted EhV_1 (*solid lines*), recombinant EhV_1 (*dashed lines*), and AviTag-EhV_1 (*dotted lines*) at 25 ± 1 °C with 10 μM, 50 μM, 100 μM, 300 μM, 1 mM, and 4 mM ATP. ATP hydrolysis was monitored as NADH oxidation in the ATP-regenerating system. The reaction was initiated by the addition of EhV_1 (final concentration of 10 nM) at 0 s. The ATP hydrolysis rate of EhV_1 was estimated from the slope of 0–10 s. *B*, *upper panel*, *red dots* indicate rotation rates determined by single-molecule rotation assay of reconstituted EhV_1. *Open red circles* indicate average rotation rates ($n \geq 3$). *Error bars* represent S.D. *Open red squares*, *open blue triangles*, and *green crosses* indicate the average of one-third of the ATP hydrolysis rates determined by the biochemical assay of reconstituted EhV_1, recombinant EhV_1, and AviTag-EhV_1, respectively ($n \geq 3$). In biochemical assay, S.D. is smaller than the size of the symbols. The *solid* and *dashed lines* indicate fits with the Michaelis-Menten equation: $V = V_{max} \times [ATP]/(K_m + [ATP])$. V_{max} = 107 ± 5 rps and K_m = 154 ± 33 μM (mean ± S.E. of fitting) were obtained by the single-molecule rotation assay for reconstituted EhV_1. V_{max} = 73 ± 2 rps and K_m = 221 ± 17 μM were obtained by the biochemical assay for reconstituted EhV_1, V_{max} = 72 ± 1 rps and K_m = 246 ± 16 μM for recombinant EhV_1, and V_{max} = 76 ± 1 rps and K_m = 300 ± 19 μM (mean ± S.E.) for AviTag-EhV_1. The apparent binding constant for ATP ($3 \times V_{max}/K_m$) was estimated as (2.2 ± 0.4) × 10^6 M^{-1} s^{-1} from the rotation assay. *Lower panel*, ratio of the rotation rate determined by the rotation assay to one-third of the ATP hydrolysis rate determined by the biochemical assay of reconstituted EhV_1.

EhV_1 Has Two Distinct Rotational States—The rotary motion of reconstituted EhV_1 was observed in a single-molecule assay using streptavidin-coated 40-nm gold colloid as a load-free probe at a rate of 1000–10,000 fps (Fig. 3). We found that the reconstituted EhV_1 complexes exhibited two distinct reversible states of rotation, namely clear and unclear (Fig. 4, *A–C*). In the clear rotational state, the majority of the centroids of gold colloid in each frame were distributed in three positions separated by 120° and were remote from the rotation center. Moreover, the time course showed clear unidirectional rotation in a counterclockwise direction (Fig. 4*A*). In contrast, in the unclear state, the centroids showed wide fluctuations toward the rotation center (Fig. 4*B*). Because the rotation rate in the unclear state seems to be similar to that in the clear state, the complex appears to rotate unidirectionally, although the measured rotation rate in the unclear state may not be accurate.

To assess whether the two rotational states are observed only in reconstituted EhV_1, the D subunit of recombinant EhV_1 was fused to AviTag, a 15-amino acid sequence that is subject to biotinylation by biotin ligase in *E. coli* (19). No differences were observed in the subunit compositions of AviTag-EhV_1 and reconstituted or recombinant EhV_1 (Fig. 1). Moreover, the ATP hydrolysis rate of AviTag-EhV_1 was comparable to that of reconstituted and recombinant EhV_1 in the biochemical assay (Fig. 2). Importantly, as was the case in the rotation assay with reconstituted EhV_1, AviTag-EhV_1 also exhibited two reversible rotational states (Fig. 4, *D–F*). This result clearly shows that the two rotational states are not an artifact of damage or inactivity caused by the reconstitution procedure but instead represent an intrinsic property of EhV_1. Given that the efficiency of biotinylation (Fig. 1) and the frequency of rotating probes for AviTag-EhV_1 were significantly lower than those for reconstituted EhV_1, we used reconstituted EhV_1 in the subsequent experiments.

Next, we analyzed the duration of the clear and unclear states for 10 μM to 40 mM ATP. Because we did not find a clear dependence of the duration on ATP concentration, we analyzed the data at various ATP concentrations collectively. The distributions of the duration times fit well to a single-exponential decay function, suggesting a single rate-limiting step in the transition between the clear and unclear states. The time constants were 0.13 ± 0.003 s (mean ± S.E. of fitting, 238 events from 58 molecules) for the clear state and 0.33 ± 0.009 s (mean ± S.E. of fitting, 199 events from 58 molecules) for the unclear state (Fig. 4, *G* and *H*). The ratio of the clear state to the total observation time was ~0.3 (=0.13/(0.13 + 0.33)).

To date, it has been unclear why transitions occur between the clear and unclear states. A study reported that although unusual fluctuations have been reported in the rotation of TtV_1 (11), the behaviors are not entirely identical; in that study (11), the authors attributed the fluctuating state to the probe adopting two orientations relative to the D subunit and excluded these data from the analysis. Alternatively, the unclear state may be due to less stable interactions between the rotor and stator in V_1 compared with those in F_1. Because V_0 and V_1 are connected not only by the rotor but also by the two peripheral stalks composed of the E and G subunits, this unstable interaction would be anticipated to occur only in the isolated V_1 complex and

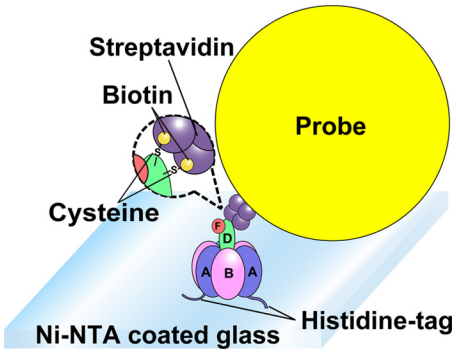

FIGURE 3. **Schematic image of the rotation assay.** Shown is the experimental setup for single-molecule rotation assay of reconstituted EhV_1. The stator A_3B_3 ring of EhV_1 was fixed on the glass surface with His_6 tag at the N termini of the A subunits. Streptavidin-coated 40-nm gold colloid was attached to biotinylated cysteine residues in the rotor DF subunit.

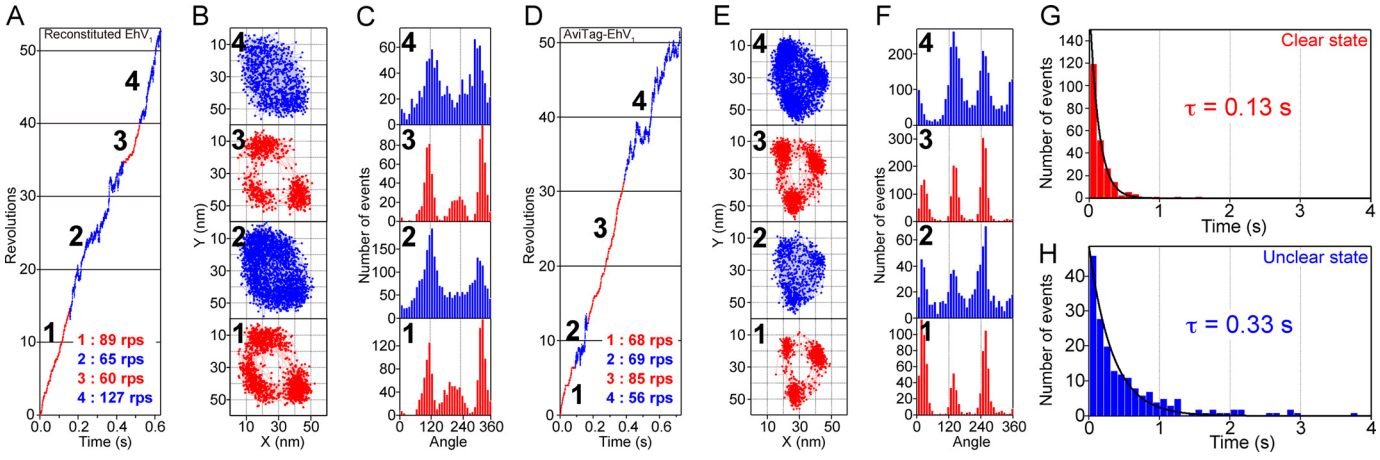

FIGURE 4. **Two distinct states in the rotation of EhV_1.** *A* and *D*, time courses of rotation, including two reversible states of single molecule-reconstituted EhV_1 (3 mM ATP) and AviTag-EhV_1 (2 mM ATP). The rotations in the clear and unclear states are highlighted in *red* and *blue*, respectively. *B* and *E*, The *x-y* trajectories of the centroid of a rotating gold colloid shown in *A* and *D*. *C* and *F*, distributions of rotary angles shown in *A* and *D*. The *numbers* in *A–C* and *D–F* indicate the corresponding parts. *G* and *H*, distributions of duration times of clear and unclear states of reconstituted EhV_1. The data at various ATP concentrations (from 10 μM to 40 mM) were analyzed collectively. The bin width was 0.1 s. The *solid curves* show the fit with single-exponential decay: constant × (exp(−*t*/τ)), where τ = 0.13 ± 0.003 s (mean ± S.E. of fitting, 238 events from 58 molecules) and 0.33 ± 0.009 s (mean ± S.E., 199 events from 58 molecules) for the clear (*G*) and unclear (*H*) states, respectively.

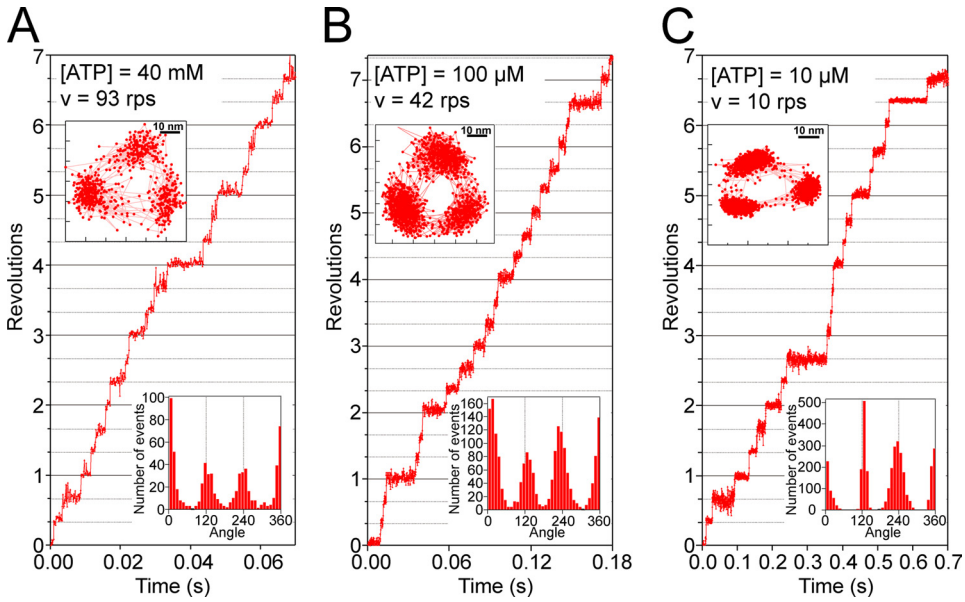

FIGURE 5. **Steps and pauses in the rotation of reconstituted EhV_1.** Shown are typical time courses of rotation of reconstituted EhV_1 at various ATP concentrations. *A*, rotation at 40 mM ATP, captured at 10,000 fps. *B*, rotation at 100 μM ATP, captured at 10,000 fps. *C*, rotation at 10 μM ATP, captured at 5000 fps. The *upper left insets* show the *x-y* trajectories of the centroid of a rotating gold colloid. The *lower right insets* show the distributions of the rotary angle.

not in the physiological V_0V_1 complex. We nevertheless concluded that the tight chemomechanical coupling of EhV_1 is achieved at least in the clear state and, accordingly, restricted our analysis in the remainder of the study to that state.

ATP Dependence of Rotation—The rotation rates of reconstituted EhV_1 were measured at various concentrations of ATP, ranging from 10 μM to 40 mM (Fig. 2*B*, *upper panel*, *red dots* and *open circles*). Below 100 μM ATP, the rotation rates were almost proportional to the ATP concentration, indicating that ATP binding is rate-limiting in this range. Above 1 mM ATP, the rotation rate was essentially constant. The rotation rates followed Michaelis-Menten kinetics with a V_{max} of 107 ± 5 rps and a K_m of 154 ± 33 μM (mean ± S.E. of fitting) (Fig. 2*B*, *upper panel*, *solid red line*). The second-order binding rate constant for ATP ($k_{on(ATP)}$) determined from $3 \times V_{max}/K_m$ was (2.2 ± 0.4) × 10^6 M^{-1} s^{-1} under the assumption that three ATP molecules were hydrolyzed per turn.

The value of K_m determined by the single-molecule rotation assay was slightly lower than that determined by the biochemical assay. Furthermore, the value of V_{max} estimated by the single-molecule rotation assay was ~50% greater than that deduced from the biochemical assay. This ratio was essentially constant at each ATP concentration (Fig. 2*B*, *lower panel*). This result may arise from inaccuracy in protein concentration determination based on the molar absorbance coefficient calculated from the amino acid sequence and/or imply that the ATP hydrolysis rate during the unclear state is slightly lower than that during the clear state. Furthermore, in the biochemical assay, the ATP hydrolysis rate gradually decreased during measurement (Fig. 2*A*). It is well known that the ATP hydrolysis of TtV_1, which functions as ATP synthase, is strongly regulated by MgADP inhibition to prevent wasteful ATP consumption (21). The ATP hydrolysis activity of TtV_1 is inhibited rapidly and irreversibly in the presence of ATP. Because the decrease in the ATP hydrolysis rate of EhV_1 was much slower than that of

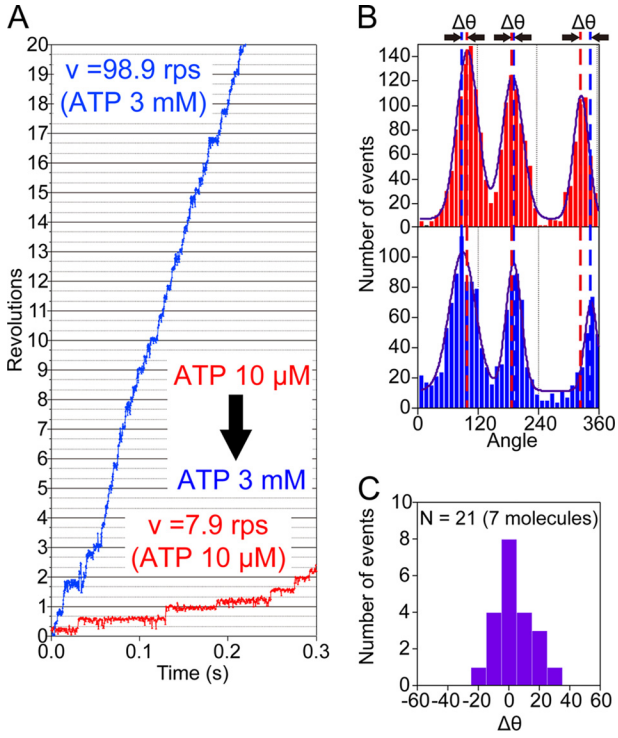

FIGURE 6. **Buffer-exchange experiments.** *A*, time courses of rotation of the same molecule at 10 μM ATP (*red*) and 3 mM ATP (*blue*). The ATP concentration was increased from 10 μM to 3 mM. *B*, distributions of the rotary angle at 10 μM ATP (*upper*) and 3 mM ATP (*lower*) shown in *A*. Δθ represents the angular differences between the pause angles (peaks) before and after buffer exchange. *C*, distribution of Δθ. The mean value was 3.2 ± 12° (mean ± S.D., 21 events from seven molecules).

TtV_1 (Fig. 2*A*) and some EhV_1 molecules showed reversible and irreversible long pauses in the rotation assay, unknown inhibited states of EhV_1 other than MgADP inhibition may exist.

Typical examples of rotation at 40 mM, 100 μM, and 10 μM ATP are shown in Fig. 5. At all ATP concentrations, EhV_1 exhibited stepwise rotation with three intervening pauses sep-

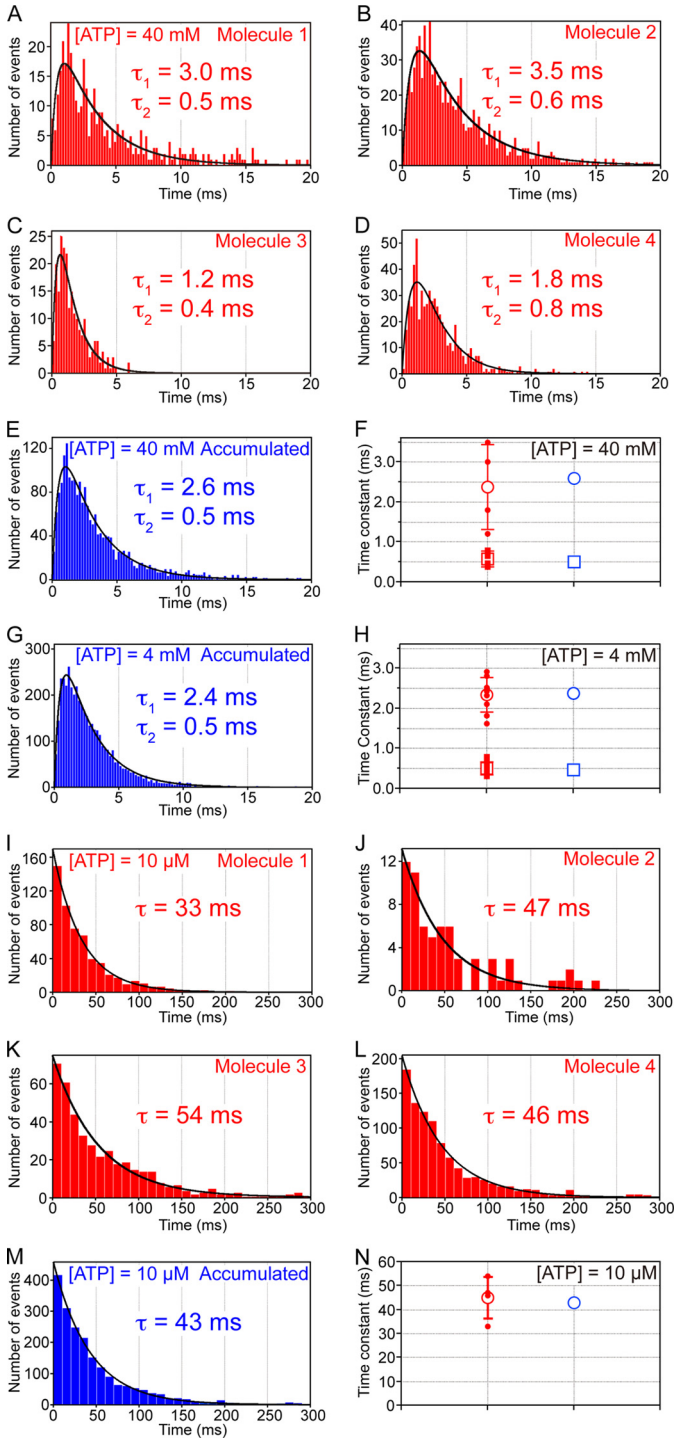

FIGURE 7. **Distributions of duration times of the pauses.** *A–D*, distributions of duration times of four single molecules at 40 mM ATP with a 0.2-ms bin width captured at 10,000 fps. The *solid curves* show fits with a model of two consecutive reactions: constant × (exp(t/τ_1) − exp(t/τ_2)), where τ_1 = 3.0 ± 0.2 ms and τ_2 = 0.5 ± 0.1 ms (mean ± S.E. of fitting, 398 events) (*A*), 3.5 ± 0.1 ms and 0.6 ± 0.04 ms (863 events) (*B*), 1.2 ± 0.2 ms and 0.4 ± 0.1 ms (228 events) (*C*), and 1.8 ± 0.3 ms and 0.8 ± 0.2 ms (608 events) (*D*). *E*, accumulated distribution of duration times of all four molecules at 40 mM. The *solid curve* shows a fit with a model of two consecutive reactions with time constants of 2.6 ± 0.1 and 0.5 ± 0.02 ms (2097 events). *F*, *red dots* and *square dots* indicate τ_1 and τ_2, respectively, shown in *A–D*. The *open red circle* and *square* indicate average τ_1 (2.4 ± 1.1 ms) and τ_2 (0.6 ± 0.2 ms) (mean ± S.D.) from four molecules. *Error bars* represent S.D. The *open blue circle* and *square* indicate τ_1 and τ_2, respectively, shown in *E*. *G*, accumulated distribution of duration times (nine molecules) at 4 mM ATP with a 0.2-ms bin width captured at 10,000 fps. The *solid curve* shows a fit with a model of two consecutive reactions: constant × (exp(t/τ_1) − exp(t/τ_2)), where τ_1 = 2.4 ± 0.05 ms and τ_2 = 0.5 ± 0.02 ms (mean ± S.E. of fitting, 4303 events). *H*, *red circles* and *square dots* indicate τ_1 and τ_2 determined by fitting the individual distributions of duration times of nine single molecules with a model of two consecutive reactions, respectively (each distribution is not shown). The *open red circle* and *square* indicate average τ_1 (2.3 ± 0.5 ms) and τ_2 (0.4 ± 0.2 ms) (mean ± S.D.) from nine molecules. *Error bars* represent S.D. The *open blue circle* and *square* indicate τ_1 and τ_2, respectively, shown in *G*. *I–L*, distributions of duration times of four single molecules at 10 μM ATP with a 10-ms bin width captured at 5000 or 2000 fps. The *solid curves* show fits with single-exponential decay: constant × (exp(−t/τ)), where τ = 33 ± 1 ms (mean ± S.E. of fitting, 581 events) (*I*), 47 ± 6 ms (67 events) (*J*), 54 ± 1 ms (432 events) (*K*), and 46 ± 1 ms (978 events) (*L*). *M*, accumulated distribution of duration times of all four molecules at 10 μM. The *solid curve* shows a fit with single-exponential decay with a time constant of 43 ± 1 ms (2058 events). *N*, the *red dots* indicate τ shown in *I–L*. The open *red circle* indicates average τ (45 ± 9 ms) (mean ± S.D.). *Error bars* represent S.D. The *open blue circle* indicates τ shown in *M*.

arated by 120°, as shown in the *x-y* trajectories and the distribution of the rotary angle (Fig. 5, *insets*). Because the 120° steps were completed within 0.2 ms (one to two frames captured at 10,000 fps), the rotation rate was determined primarily by the duration of the intervening pause. At 40 mM ATP, a concentration considerably higher than the K_m, the intervening pauses would represent the catalytic pauses (Fig. 5*A*) because the expected binding time constant for ATP (0.011 ms, estimated from $1/(40 \times 10^{-3}\ \text{M} \times 2.2 \times 10^{6}\ \text{M}^{-1}\ \text{s}^{-1})$) was 100-fold smaller than the duration times (3.1 ms) of pauses expected from the V_{max} (1/(107 × 3)). At 10 μM ATP, a concentration substantially lower than the K_m, the intervening pauses would correspond to the ATP-waiting pauses because ATP binding is rate-limiting under these conditions (Fig. 5*C*).

Even at 100 μM ATP, a concentration near the K_m and at which the duration of the ATP-waiting pause approaches that of the catalytic pause, EhV_1 exhibited only three pauses separated by 120° (Fig. 5*B*). This finding suggests that there are no substeps in the rotation of EhV_1, as is the case for TtV_1 (10, 11).

Buffer-exchange Experiment—To further confirm that the angles of the ATP-waiting pauses observed at low ATP concentrations correspond to those of the catalytic pauses observed at saturating ATP concentrations, we next conducted a buffer-exchange experiment. After recording the stepwise rotation of EhV_1 pausing every 120° at 10 μM ATP, we increased the ATP concentration to 3 mM by infusing buffer containing 3 mM ATP into the flow cell. After buffer exchange, although the rotation rate increased significantly, EhV_1 continued to rotate with discrete 120° steps, pausing at almost the same angles (Fig. 6, *A* and *B*). The distributions of the rotary angles indicated three peaks corresponding to three pauses in the rotation (Fig. 6*B*). To assess the difference in the angular position ($\Delta\theta$) between 10 μM and 3 mM ATP, the positions of the peaks were determined by fitting the histogram with Gaussian functions and then comparing them with the nearest ones (Fig. 6*B*). The distribution of $\Delta\theta$ showed a single peak around 0°, with a mean value of 3.2 ± 12° (mean ± S.D., 21 events from seven molecules) (Fig. 6*C*). On the basis of these data, we confirmed again that the rotation of EhV_1 contains no substeps.

Dwell Time Analysis—To obtain the time constants and kinetic parameters for elementary reaction steps such as ATP binding, ATP cleavage, and product release, we analyzed the duration of the pauses. On analyzing four molecules at saturating ATP concentrations (40 mM), all distributions of the durations of the catalytic pauses showed a convex shape (Fig. 7, *A–D*). At 40 mM

TABLE 1
Kinetic parameters of V_1-ATPases and F_1-ATPases from different sources

Protein/measurement temperature	$k_{on(ATP)}$[a]	$k_{on(ATP)}$ ($3 \times V_{max}/K_m$)[b]	τ_1/τ_2[c]	Ref.
	$M^{-1} s^{-1}$	$M^{-1} s^{-1}$	*ms*	
EhV_1[d]				
26 ± 1 °C	(2.3 ± 0.03) × 10^6	(2.2 ± 0.4) × 10^6	2.6 ± 0.1/0.5 ± 0.02[e]	This work
TtV_1				
23 °C	1.5 × 10^6	0.84 × 10^6	2.8/2.8	11
24 ± 1 °C		1.39 × 10^6		21
TF_1				
23 °C	3.0 × 10^7	2.6 × 10^7	1.6/0.71	13
25 ± 1 °C			1.34/0.29	20
25 ± 1 °C		2.2 × 10^7		27
EF_1				
23 °C	4.7 × 10^7	6.4 × 10^7	0.41/0.29	15

[a] The second-order binding rate constant for ATP ($k_{on(ATP)}$) was determined from the distribution of the duration of the ATP-waiting pause.
[b] The second-order binding rate constant for ATP ($k_{on(ATP)}$) was determined from $3 \times V_{max}/K_m$.
[c] Time constants were determined from the distribution of the duration of the catalytic pause, which corresponds to ATP cleavage and either ADP or phosphate release (or both).
[d] The values are the mean ± S.E. of fitting.
[e] The values were obtained at 40 mM ATP.

ATP, the expected time constant for ATP binding (0.011 ms) was too short to be resolved. Therefore, three elementary reaction steps could occur during the catalytic pauses, namely ATP cleavage, ADP release, and phosphate release. We first attempted to fit the distributions with a model of three consecutive reactions. This failed to improve the fits compared with a model of two consecutive reactions with two time constants. The average time constants from four molecules were 2.4 ± 1.1 and 0.6 ± 0.2 ms (mean ± S.D.) (Fig. 7*F*, *open red circle* and *square*). These values are consistent with the time constants of 2.6 ± 0.1 and 0.5 ± 0.02 ms (mean ± S.E. of fitting, 2097 events) determined by reproducing the accumulated distribution of the pause duration time from all four molecules (Fig. 7*E*). In addition, at 4 mM ATP (the expected time constant for ATP binding is 0.11 ms), similar accumulated distribution and time constants of 2.4 ± 0.05 and 0.5 ± 0.02 ms (mean ± S.E. of fitting, 4303 events from nine molecules) were obtained (Fig. 7, *G* and *H*), consistent with the saturation of the rotation rate at this concentration (Fig. 2*B*).

These time constants would correspond to (i) ATP cleavage and (ii) ADP and/or phosphate release, although it is currently unclear which time constant corresponds to which elementary reaction step. At a low ATP concentration (10 μM), as discussed above, the duration of the pauses corresponded to that of ATP waiting. Analysis of the four molecules showed that the distributions of the ATP-waiting duration time followed single-exponential decay (Fig. 7, *I–L*), indicating that EhV_1 consumed one ATP molecule/120° step. The average time constant from four molecules was 45 ± 9 ms (mean ± S.D.) (Fig. 7*N*, *open red circle*), which is consistent with a time constant of 43 ± 1 ms (mean ± S.E. of fitting, 2058 events) determined by reproducing the accumulated distribution of the duration time from all four molecules (Fig. 7*M*). This value corresponds to a $k_{on(ATP)}$ of (2.3 ± 0.03) × 10^6 M^{-1} s^{-1}, which is consistent with that determined by $3 \times V_{max}/K_m$ ((2.2 ± 0.4) × 10^6 M^{-1} s^{-1}), shown in Fig. 2*B*.

DISCUSSION

In this study, using a single-molecule assay, we have shown that EhV_1 is a rotary molecular motor. To our knowledge, this is the first report showing that a eubacterial V_1 functions as an ATP-driven ion pump under physiological conditions. EhV_1 exhibited two rotational states, namely clear and unclear (Fig. 4). Assuming that the clear rotational state represents the tight chemomechanical coupling of EhV_1, we analyzed this state to elucidate the basic rotational properties of EhV_1. Our hypothesis that the unclear state is caused by unstable interactions between the rotor and stator of EhV_1 must be examined by rotation assay of the entire *E. hirae* V-ATPase complex, in which the interactions between the rotor and stator are stabilized by two peripheral stalks. To perform this study, we are currently designing an *E. coli* expression system in which an appropriately tagged recombinant V-ATPase complex can be produced for a rotation assay.

In the clear rotational state, at all ATP concentrations ranging from below to above the K_m, EhV_1 rotated unidirectionally in a counterclockwise direction, exhibiting three pauses separated by 120° (Fig. 5). No substeps were resolved, as has been reported for TtV_1 (10, 11). In contrast, in the region of their respective K_m values, TF_1 and EF_1 have been reported to rotate with six pauses/turn (13–15). Recently, the overall crystal structures of TtV_1 and EhV_1 were shown to be similar (4–7), especially with respect to the interaction sites between the rotor and stator. These structures are distinct from the structure of F_1 (22), although many amino acid residues associated with catalysis in the binding pocket are conserved between V_1 and F_1. These results imply that the degree of similarity in the interactions between the rotor and stator determines the presence or absence of substeps in the rotation.

Table 1 contains a comparison of the kinetic parameters determined by the single-molecule assay for EhV_1, showing values for TtV_1, TF_1, and EF_1. Despite the difference in physiological function between EhV_1 and TtV_1 and notwithstanding the large difference (>30 °C) in the optimal growth temperatures between *E. hirae* and *T. thermophilus*, the values for EhV_1 are closer to those for TtV_1 than for TF_1 and EF_1. This result implies that the basic properties of rotary dynamics are determined by their overall structures and that the difference in the physiological function derives from regulatory mechanisms such as MgADP inhibition.

During the unclear rotational state, the centroids of the gold colloid showed wide fluctuations toward the rotation center. It should be noted that EhV_1 nevertheless rotated unidirectionally, implying that even if the interactions between the rotor and stator are not perfect, EhV_1 maintains unidirectional and cooperative rotary catalysis. Recently, rotary catalysis of the rotor-less stator $\alpha_3\beta_3$ ring of TF_1 was demonstrated by high-speed atomic force microscopy (23), and we speculate that the stator A_3B_3 ring also likely exhibits rotary catalysis in the absence of the rotor DF subunits.

The chemomechanical coupling scheme of TF_1 has been extensively studied by advanced single-molecule techniques such as a rotation assay of hybrid molecules and single-molecule manipulation with magnetic tweezers (24–26). For a single catalytic site of TF_1, after ATP binding at 0°, ATP cleavage, ADP release, and phosphate release occur at 200°, 240°, and 320°, respectively (26). Further studies on EhV_1 using advanced single-molecule techniques and high-resolution structural analysis will provide details on its chemomechanical coupling scheme. Moreover, comparison of the schemes of V_1 and F_1 from various species will shed light on the general mechanism of rotary molecular motors.

Acknowledgments—We thank Mio Inoue and Ken Ishii for preparation of the plasmids and Shoichi Toyabe for providing the data analysis software. We also thank all members of the laboratory for valuable discussions and comments.

REFERENCES

1. Nishi, T., and Forgac, M. (2002) The vacuolar (H^+)-ATPases–nature's most versatile proton pumps. *Nat. Rev. Mol. Cell Biol.* **3,** 94–103
2. Forgac, M. (2007) Vacuolar ATPases: rotary proton pumps in physiology and pathophysiology. *Nat. Rev. Mol. Cell Biol.* **8,** 917–929
3. Marshansky, V., and Futai, M. (2008) The V-type H^+-ATPase in vesicular trafficking: targeting, regulation and function. *Curr. Opin. Cell Biol.* **20,** 415–426
4. Numoto, N., Hasegawa, Y., Takeda, K., and Miki, K. (2009) Inter-subunit interaction and quaternary rearrangement defined by the central stalk of prokaryotic V_1-ATPase. *EMBO Rep.* **10,** 1228–1234
5. Maher, M. J., Akimoto, S., Iwata, M., Nagata, K., Hori, Y., Yoshida, M., Yokoyama, S., Iwata, S., and Yokoyama, K. (2009) Crystal structure of A_3B_3 complex of V-ATPase from *Thermus thermophilus*. *EMBO J.* **28,** 3771–3779
6. Arai, S., Saijo, S., Suzuki, K., Mizutani, K., Kakinuma, Y., Ishizuka-Katsura, Y., Ohsawa, N., Terada, T., Shirouzu, M., Yokoyama, S., Iwata, S., Yamato, I., and Murata, T. (2013) Rotation mechanism of *Enterococcus hirae* V_1-ATPase based on asymmetric crystal structures. *Nature* **493,** 703–707
7. Nagamatsu, Y., Takeda, K., Kuranaga, T., Numoto, N., and Miki, K. (2013) Origin of asymmetry at the intersubunit interfaces of V-ATPase from *Thermus thermophilus*. *J. Mol. Biol.* **425,** 2699–2708
8. Imamura, H., Nakano, M., Noji, H., Muneyuki, E., Ohkuma, S., Yoshida, M., and Yokoyama, K. (2003) Evidence for rotation of V_1-ATPase. *Proc. Natl. Acad. Sci. U.S.A.* **100,** 2312–2315
9. Hirata, T., Iwamoto-Kihara, A., Sun-Wada, G. H., Okajima, T., Wada, Y., and Futai, M. (2003) Subunit rotation of vacuolar-type proton pumping ATPase: relative rotation of the G and C subunits. *J. Biol. Chem.* **278,** 23714–23719
10. Imamura, H., Takeda, M., Funamoto, S., Shimabukuro, K., Yoshida, M., and Yokoyama, K. (2005) Rotation scheme of V_1-motor is different from that of F_1-motor. *Proc. Natl. Acad. Sci. U.S.A.* **102,** 17929–17933
11. Furuike, S., Nakano, M., Adachi, K., Noji, H., Kinosita, K., Jr., and Yokoyama, K. (2011) Resolving stepping rotation in *Thermus thermophilus* H^+-ATPase/synthase with an essentially drag-free probe. *Nat. Commun.* **2,** 233
12. Iino, R., and Noji, H. (2013) Operation mechanism of F_oF_1-adenosine triphosphate synthase revealed by its structure and dynamics. *IUBMB Life* **65,** 238–246
13. Yasuda, R., Noji, H., Yoshida, M., Kinosita, K., Jr., and Itoh, H. (2001) Resolution of distinct rotational substeps by submillisecond kinetic analysis of F_1-ATPase. *Nature* **410,** 898–904
14. Shimabukuro, K., Yasuda, R., Muneyuki, E., Hara, K. Y., Kinosita, K., Jr., and Yoshida, M. (2003) Catalysis and rotation of F_1 motor: cleavage of ATP at the catalytic site occurs in 1 ms before 40° substep rotation. *Proc. Natl. Acad. Sci. U.S.A.* **100,** 14731–14736
15. Bilyard, T., Nakanishi-Matsui, M., Steel, B. C., Pilizota, T., Nord, A. L., Hosokawa, H., Futai, M., and Berry, R. M. (2013) High-resolution single-molecule characterization of the enzymatic states in *Escherichia coli* F_1-ATPase. *Philos. Trans. R. Soc. Lond. B Biol. Sci.* **368,** 20120023
16. Kakinuma, Y., and Igarashi, K. (1994) Purification and characterization of the catalytic moiety of vacuolar-type Na^+-ATPase from *Enterococcus hirae*. *J. Biochem.* **116,** 1302–1308
17. Murata, T., Takase, K., Yamato, I., Igarashi, K., and Kakinuma, Y. (1997) Purification and reconstitution of Na^+-translocating vacuolar ATPase from *Enterococcus hirae*. *J. Biol. Chem.* **272,** 24885–24890
18. Suzuki, T., Ueno, H., Mitome, N., Suzuki, J., and Yoshida, M. (2002) F_0 of ATP synthase is a rotary proton channel. Obligatory coupling of proton translocation with rotation of *c*-subunit ring. *J. Biol. Chem.* **277,** 13281–13285
19. Beckett, D., Kovaleva, E., and Schatz, P. J. (1999) A minimal peptide substrate in biotin holoenzyme synthetase-catalyzed biotinylation. *Protein Sci.* **8,** 921–929
20. Ueno, H., Nishikawa, S., Iino, R., Tabata, K. V., Sakakihara, S., Yanagida, T., and Noji, H. (2010) Simple dark-field microscopy with nanometer spatial precision and microsecond temporal resolution. *Biophys. J.* **98,** 2014–2023
21. Uner, N. E., Nishikawa, Y., Okuno, D., Nakano, M., Yokoyama, K., and Noji, H. (2012) Single-molecule analysis of inhibitory pausing states of V_1-ATPase. *J. Biol. Chem.* **287,** 28327–28335
22. Abrahams, J. P., Leslie, A. G., Lutter, R., and Walker, J. E. (1994) Structure at 2.8 Å resolution of F_1-ATPase from bovine heart mitochondria. *Nature* **370,** 621–628
23. Uchihashi, T., Iino, R., Ando, T., and Noji, H. (2011) High-speed atomic force microscopy reveals rotary catalysis of rotorless F_1-ATPase. *Science* **333,** 755–758
24. Ariga, T., Muneyuki, E., and Yoshida, M. (2007) F_1-ATPase rotates by an asymmetric, sequential mechanism using all three catalytic subunits. *Nat. Struct. Mol. Biol.* **14,** 841–846
25. Adachi, K., Oiwa, K., Nishizaka, T., Furuike, S., Noji, H., Itoh, H., Yoshida, M., and Kinosita, K., Jr. (2007) Coupling of rotation and catalysis in F_1-ATPase revealed by single-molecule imaging and manipulation. *Cell* **130,** 309–321
26. Watanabe, R., Iino, R., and Noji, H. (2010) Phosphate release in F_1-ATPase catalytic cycle follows ADP release. *Nat. Chem. Biol.* **6,** 814–820
27. Tanigawara, M., Tabata, K. V., Ito, Y., Ito, J., Watanabe, R., Ueno, H., Ikeguchi, M., and Noji, H. (2012) Role of the DELSEED loop in torque transmission of F_1-ATPase. *Biophys. J.* **103,** 970–978